Transmission of a detonation wave across an inert layer

Kelsey C. Tang-Yuk[1*], XiaoCheng Mi[1], John H.S. Lee[1], Hoi Dick Ng[2], Ralf Deiterding[3]

[1]Department of Mechanical Engineering, McGill University,
Montreal H3A 0C3, Canada.
[2]Department of Mechanical, Industrial and Aerospace Engineering, Concordia University,
Montreal H3G 1M8, Canada.
[3]Aerodynamics and Flight Mechanics Research Group, University of Southampton,
Southampton SO171BJ, United Kingdom.

*Correspondence to: kelsey.tangyuk@mail.mcgill.ca

Abstract

The transmission of a detonation wave across a layer of inert gas is studied via one- and two-dimensional numerical simulations based on the reactive Euler equations. The resulting transient transmission process from the one-dimensional simulations is first explored in detail, and is analyzed via distance-time characteristic diagrams. The physics of this transient process is the same until the end of a quasi-steady period. Afterward, the energy release from the combustion may couple to the gas dynamics. Through this coupling, the pressure pulse accompanying the energy release can be rapidly amplified, and consequently, leads to detonation onset. If the inert layer is too thick, the detonation cannot be successfully re-initiated downstream. This inert-layer thickness beyond which a detonation fails to be re-initiated is determined as the critical thickness, $\delta_{\mathrm{i,cr}}$. The mechanisms underlying the scenarios with a successful and unsuccessful re-initiation are demonstrated in detail. A parametric study considering simplified and detailed chemical kinetics (i.e., a stoichiometric mixture of hydrogen and air at various initial pressure from 0.1-$1\ \mathrm{atm}$) demonstrate that $\delta_{\mathrm{i,cr}}$ normalized by the intrinsic ZND induction length, Δ_{I}, asymptotically decreases with an increase of the effective activation energy, E_{a}. The one-dimensional simulations under-predict the experimental results [1, 2] of $\delta_{\mathrm{i,cr}}/\Delta_{\mathrm{I}}$ by at least one order of magnitude. In the two-dimensional scenarios, transverse-wave instabilities are present and allow the detonation wave to re-initiate in cases where re-initiation is unsuccessful in one dimension. The two-dimensional results of $\delta_{\mathrm{i,cr}}$ are in a closer agreement with the experimental findings.

Keywords– Detonation transmission; Inert layer; Detonation onset; Numerical simulation

1 Introduction

Detonation research has focused mainly on uniform mixtures. However, the propagation of detonation waves in non-uniform mixtures is of both practical and fundamental interest. In terms of the fundamental aspect, studying the transient response can help to elucidate the detonation propagation and onset mechanism. On the practical side, in accidental vapor cloud explosions, dispersion and mixing of the fuel and air will invariably lead to a highly inhomogeneous mixture. There can be variations in thermodynamic state such as density, and variations in mixture composition such as pockets of unmixed air embedded in the cloud. In previous work, the transmission of a detonation wave across an interface with an abrupt change in thermodynamic state (i.e., density and temperature) was investigated [3]. The present study is concerned specifically with the transmission of a detonation wave across a pocket of inert gas.

A layer of inert gas is embedded in an otherwise uniform reactive gas as shown in Fig. 1. When a detonation enters the inert layer, there will be a reduction in the energy release from chemical reactions. This reduction will cause the detonation to decay, with the leading shock separating from the reaction zone. Therefore, the leading shock will be attenuated as it emerges from the inert layer, with the amplitude of this transmitted shock depending

on the thickness of the inert layer. If the inert layer is sufficiently thin, i.e., the transmitted shock is sufficiently strong, ignition of the downstream[1] reactive mixture will occur. If the subsequent reaction rate is sufficiently rapid, the shock will accelerate, resulting in a re-initiation of a detonation wave. Therefore, there will be a critical thickness in which ignition and acceleration of the shock lead to the onset of a detonation. The present study attempts to determine the critical thickness for the re-initiation of detonation downstream of the inert layer via one and two-dimensional computational analysis.

There have been a few previous studies on the transmission of a detonation across an inert layer. Bull *et al*. [1] investigated the transmission of detonation waves in stoichiometric propane-air and ethylene-air mixtures across an inert air gap. The mixtures were contained in polythene bags, and the reactive sections were separated from the air gap by thin Melinex diaphragms which were withdrawn just prior to detonation initiation. A microwave interferometer monitored the detonation velocity, and piezoelectric transducers recorded the time of arrival and the magnitude of the detonation pressure. In addition, detonation occurrence was indicated by the size of the polythene bag fragments. Detonation was found to re-initiate across an air layer less than $0.15\,\mathrm{m}$ for the ethylene-air and $0.12\,\mathrm{m}$ for the propane-air.

Similar studies were later carried out by Bjerketvedt, Engebretsen and colleagues [2, 4]. They used a square detonation tube of internal dimension of $125\,\mathrm{mm}$, containing an air section either 100, 150 or $200\,\mathrm{mm}$ long. The air section was separated from the reactive sections by slide valves which were rapidly removed just prior to the experiment. With the prescribed air gap of 0.1-$0.2\,\mathrm{m}$, detonation was successfully re-initiated for stoichiometric acetylene-air, but not for ethylene-air. Pressure transducer records showed a build-up of pressure and then the onset of a detonation immediately behind the transmitted shock. Gavrilenko *et al*. [5] and Teodorczyk *et al*. [6] have also performed similar experiments with slight variations in introducing an inert layer. Gavrilenko *et al*. [5] used rubber membranes to separate the reactive and inert gases, which were punctured prior to the experiment; whereas Teodorczyk *et al*. [6] injected an inert gas into a channel filled with a reactive gas.

In all of the previous studies, it is clear that obtaining a well-defined boundary between the reactive mixture and inert gas is an experimental challenge. Initially, the gases must be separated by some means such as a diaphragm or slide valve. Removal of this separator invariably generates turbulence, causing mixing and a zone of variable composition at the boundary of the layer to be developed. For example, in the experiments of Bjerketvedt *et al*. [2] the mixing zone created after removal of the slide valves was found to be approximately $30\,\mathrm{mm}$ wide, which is fairly large compared to the length of the inert section.

A recent numerical study by Wang *et al*. [7] considered both a single inert layer as well as a series of inert layers. One and two-dimensional simulations were performed. The reactive mixture was stoichiometric hydrogen-oxygen-nitrogen and the inert gas was pure nitrogen. A critical thickness of $0.15\,\mathrm{mm}$ was found for the one-dimensional case. For the two-dimensional case, a critical thickness of $0.37\,\mathrm{mm}$ was reported for a series of inert layers with spacing of $2\,\mathrm{mm}$. It is of interest to note that these critical thicknesses are about two orders of magnitude smaller than the experimentally observed values. In another recent numerical study, Tropin and Bedarev [8] looked at the effect of different inert species (CO_2, N_2 and Ar), where the reactive mixture was hydrogen and air. Nevertheless this work is geared toward hazard prevention, and has not illustrated the details of the transmission process.

Overall, the studies thus far have allowed for only a few inert lengths [2, 4] or only a couple of reactive mixtures [1, 7, 8]. Therefore, the dependence of the critical inert thickness on the reactive mixture has not been thoroughly explored. The critical thickness should be characteristic of a reactive mixture, and may therefore provide a length scale to describe the detonability of the mixture. Typically, detonation cell size is the length scale used to describe detonability. However, detonation cell size is irregular and its measurement by the soot foil technique is subjective. In addition, cell size cannot in general be used exclusively; cell regularity (or mixture stability) is also important [9–11]. The present study is computational which facilitates a parametric study as mixture parameters can be more readily varied. In addition, numerical simulation avoids the problem of mixing between reactive and inert gases allowing the inert boundaries to be well defined.

2 Problem description

2.1 Governing equations

For simplicity, the problem is assumed to be one or two-dimensional, and viscous transport and heat conduction are neglected. In addition, the initial pressure and temperature are uniform throughout the domain. The governing

[1] "Downstream" means ahead of the leading shock wave of an incident detonation. In the reported simulations in this paper, as the incident detonation propagates rightwards, "upstream" and "downstream" mean towards the left and right ends of the domain, respectively.

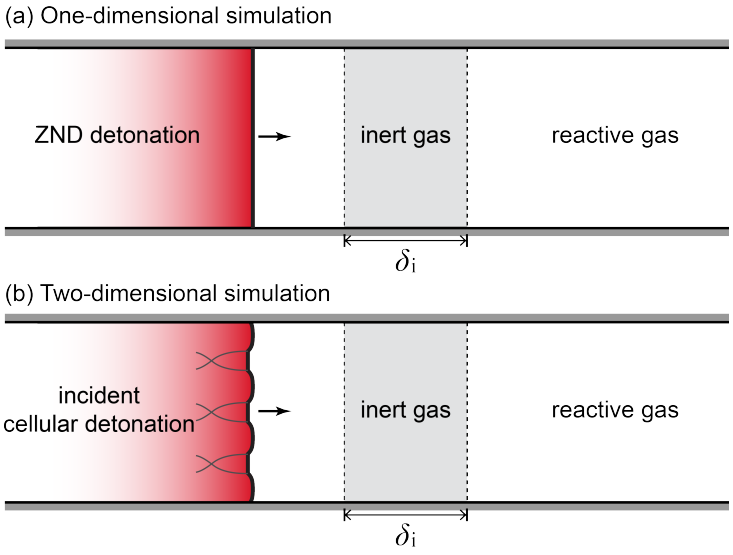

Figure 1: Schematic illustration showing the problem of an incident detonation wave propagating towards a layer of inert gas with a thickness of δ_i: **(a)** One-dimensional simulation with an planar incident detonation wave based on the ZND structure; **(b)** Two-dimensional simulation subjected to an incident detonation wave with a fully developed cellular structure.

equations are the one or two-dimensional, inviscid Euler equations with reactive source terms, describing the conservation of mass, momentum and energy. That is,

$$\frac{\partial \mathbf{U}}{\partial \tilde{t}} + \frac{\partial \mathbf{F}(\mathbf{U})}{\partial \tilde{x}} + \frac{\partial \mathbf{G}(\mathbf{U})}{\partial \tilde{y}} = \mathbf{S}(\mathbf{U}) \tag{1}$$

with conserved variables $\mathbf{U}$, convective fluxes $\mathbf{F}(\mathbf{U})$ and $\mathbf{G}(\mathbf{U})$, and source terms $\mathbf{S}(\mathbf{U})$ given by,

$$\begin{aligned} \mathbf{U} &= (\tilde{\rho}, \tilde{\rho}\tilde{u}, \tilde{\rho}\tilde{v}, \tilde{\rho}\tilde{e}, \tilde{\rho}Y_n)^T \\ \mathbf{F}(\mathbf{U}) &= (\tilde{\rho}\tilde{u}, \tilde{\rho}\tilde{u}^2 + \tilde{p}, \tilde{\rho}\tilde{u}\tilde{v}, \tilde{u}(\tilde{\rho}\tilde{e} + \tilde{p}), \tilde{\rho}\tilde{u}Y_n)^T \\ \mathbf{G}(\mathbf{U}) &= (\tilde{\rho}\tilde{v}, \tilde{\rho}\tilde{u}\tilde{v}, \tilde{\rho}\tilde{v}^2 + \tilde{p}, \tilde{v}(\tilde{\rho}\tilde{e} + \tilde{p}), \tilde{\rho}\tilde{v}Y_n)^T \\ \mathbf{S}(\mathbf{U}) &= (0, 0, 0, 0, \tilde{\omega_n})^T. \end{aligned} \tag{2}$$

Here $\tilde{\rho}$, $\tilde{u}$, $\tilde{v}$, $\tilde{p}$, $\tilde{e}$ are the density, particle velocities in x and y directions, pressure and specific total energy, respectively. The chemical species are represented by subscript n, where Y_n are their mass fractions, and $\tilde{\omega_n}$ their production rates. In the present study three different chemical kinetic models are used which will be described in turn.

2.1.1 Three-step chemical kinetic model

For the majority of the study, a three-species, three-step reaction model was used to represent features of chain branching kinetics. This model has been used in previous studies [12–15]. A calorically perfect gas with a constant ratio of specific heats γ is assumed, and dimensionless quantities are defined as,

$$\begin{aligned} p &= \frac{\tilde{p}}{\gamma \tilde{p}_0}, \quad \rho = \frac{\tilde{\rho}}{\tilde{\rho}_0}, \quad T = \frac{\tilde{T}}{\gamma \tilde{T}_0}, \\ u &= \frac{\tilde{u}}{\tilde{c}_0}, \quad e = \frac{p}{(\gamma - 1)\rho} + \frac{u^2}{2} - q \end{aligned} \tag{3}$$

where q is the local heat released by combustion, and c is the sound speed. The tilde denotes a dimensional quantity, and the subscript 0 refers to the initial unburnt state.

The three species are fuel, radical and product, which are denoted F, R and Z, respectively. The chain initiating reaction is represented by F $\rightarrow$ R, the chain branching reaction by F + R $\rightarrow$ 2R, and the chain terminating reaction

by R $\rightarrow$ Z. The initiating and branching reaction rates have a dependence on temperature of an Arrhenius form, and the chain terminating reaction is assumed to be independent of temperature. The system of equations is,

$$\frac{\mathrm{d}(\rho f)}{\mathrm{d}t} = -(\omega_A + \omega_B), \quad \frac{\mathrm{d}(\rho r)}{\mathrm{d}t} = \omega_A + \omega_B - \omega_C \tag{4}$$

with,

$$\omega_A = \rho f \exp\left[E_A\left(\frac{1}{T_A} - \frac{1}{T}\right)\right], \quad \omega_B = \rho f r \exp\left[E_B\left(\frac{1}{T_B} - \frac{1}{T}\right)\right], \quad \omega_C = \rho r \tag{5}$$

where f and r are the mass fractions of fuel and radical species, and ω_A, ω_B and ω_C are the chain initiating, branching and terminating reaction rates. E_A and E_B are the activation energies of the chain initiating and chain branching reactions, respectively, and T_A and T_B are their crossover temperatures. The initiating and branching reactions are assumed to be thermally neutral, such that only the chain terminating reaction is exothermic. Thus the local chemical energy release, q is,

$$q = Q(1 - f - r) = Qz \tag{6}$$

where z is the product mass fraction, and Q is the total chemical energy released per unit mass. The activation energies have been non-dimensionalized as follows,

$$E_A = \frac{\tilde{E_A}}{\tilde{c_0}^2}, \quad E_B = \frac{\tilde{E_B}}{\tilde{c_0}^2}. \tag{7}$$

To be consistent with the literature for this model, for example [13, 14], the rate constant of the chain terminating reaction (ω_C in Eq. 5) is set equal to unity, which defines the reference time scale $\tilde{t}_{\mathrm{ref}}$. Then, the reference length scale is the reference time scale multiplied by the sound speed in the undisturbed reactant ($\tilde{l}_{\mathrm{ref}} = \tilde{c}_0\tilde{t}_{\mathrm{ref}}$).

In order to represent real chain branching reactions, the kinetic parameters must satisfy,

$$T_A > T_{\mathrm{vN}}, \quad T_B < T_{\mathrm{vN}}, \quad E_B \ll E_A \tag{8}$$

where T_{vN} is the von Neumann shock temperature [12, 13]. These criteria are based on the fact that the initiating reaction generally requires a large activation energy to break the relatively strong bonds of the fuel, whereas the branching reaction generally requires less energy. In addition, the chain branching reaction is the most critical reaction in systems with chain branching chemistry [16]. Therefore, both of the chain branching parameters, namely the crossover temperature, T_B and the activation energy, E_B are varied. In the present study, $T_B = 0.84$-$0.95T_{\mathrm{vN}}$, $E_B = 10$ or 15, $T_A = 3T_{\mathrm{vN}}$, and $E_A = 37.5$. These modelling values are chosen not only to be within typical values for detonable mixtures [13], but also for which the detonation can either propagate steadily or exhibit unstable propagation dynamics.

2.1.2 Two-step chemical kinetic model

A simpler two-step chemical kinetic model is used for comparison, which has also been used in previous studies [3, 17]. Equivalent two-step kinetic models have also been used recently to clarify the role of separate induction and reaction zones on the nonlinear dynamics of pulsating detonations [18, 19]. Dimensionless quantities can be defined as before (Eq. 3). The reaction is split into a thermally neutral induction stage and a reaction stage. Both stages have a temperature-sensitive Arrhenius form of the reaction rate. The system of equations is,

$$\begin{aligned} \frac{\mathrm{d}(\rho\xi)}{\mathrm{d}t} &= H(1-\xi)\rho k_{\mathrm{I}} \exp\left[E_{\mathrm{I}}\left(\frac{1}{T_{\mathrm{vN}}} - \frac{1}{T}\right)\right], \\ \frac{\mathrm{d}(\rho\lambda)}{\mathrm{d}t} &= (1 - H(1-\xi))\rho k_{\mathrm{R}}(1-\lambda)\exp\left(\frac{-E_{\mathrm{R}}}{T}\right) \end{aligned} \tag{9}$$

with the step function,

$$H(1-\xi) = \begin{cases} 1 & \xi < 1 \\ 0 & \xi \geq 1. \end{cases} \tag{10}$$

Here ξ is progress variable, so that at the end of the induction process all of the fuel is converted to radicals instantaneously. Then λ can be thought of as the mass fraction of product. The parameters k_{I} and k_{R} are rate constants, and E_{I} and E_{R} are activation energies for the induction and reaction steps, respectively. Thus, the local chemical energy release, q is now,

$$q = \lambda Q. \tag{11}$$

Again, activation energies can be non-dimensionalized as above (Eq. 7), i.e.,

$$E_{\mathrm{I}} = \frac{\tilde{E}_{\mathrm{I}}}{\tilde{c}_0{}^2}, \quad E_{\mathrm{R}} = \frac{\tilde{E}_{\mathrm{R}}}{\tilde{c}_0{}^2}. \tag{12}$$

In addition, the rate constant $k_{\mathrm{I}} = -u_{\mathrm{vN}}$, where u_{vN} is the von Neumann particle velocity in the shock fixed frame. This defines the length and time scales so that the Zel'dovich-von Neumann-Döring (ZND) induction length is unity [17]. The activation energy of the induction step is generally much larger than the reaction step, i.e.,

$$E_{\mathrm{I}} \gg E_{\mathrm{R}}. \tag{13}$$

Again this is because it involves breaking the relatively strong fuel bonds, and since this is the most crucial step E_{I} is varied. In the present study for the one-dimensional simulations, the rate constant $k_{\mathrm{R}} = 0.8$ or 1, the activation energy $E_{\mathrm{R}} = T_{\mathrm{vN}}$, and the activation energy of the induction, $E_{\mathrm{I}} = 6\text{-}10T_{\mathrm{vN}}$. For the two-dimensional simulations, this two-step kinetic model was used exclusively to minimize computational expense. The rate constant $k_{\mathrm{R}} = 0.8$, the activation energy $E_{\mathrm{R}} = T_{\mathrm{vN}}$, and the activation energy of the induction, $E_{\mathrm{I}} = 9\text{-}13T_{\mathrm{vN}}$.

2.1.3 Detailed chemical kinetic model

Finally, a detailed chemical kinetic mechanism for hydrogen-air combustion is used. The mechanism is a subset of the hydrocarbon kinetic mechanism of Westbrook [20]. There are 34 elementary reactions and 9 species, including H_2, O_2, H, O, OH, H_2O, HO_2, H_2O_2 and N_2. The combustible mixture is always stoichiometric hydrogen-air, while the inert layer is always air. The initial temperature throughout the domain is 295 K, and the initial pressure is varied from 0.1-1 atm.

2.2 Generalized parameters

The chemical kinetic parameters described above are specific to each model, but might be more useful in a general form that is applicable to all models. For any detonable gas there are three universal governing parameters [21]. These parameters are the induction time/length scale, the activation energy, and the thermal energy release.

2.2.1 Induction length

For a two-step chemical kinetic model, the induction length can be clearly defined in the ZND detonation structure and used to non-dimensionalize the length scales of the problem. For three-step and detailed chemical kinetic models, there is no standard definition of induction length. However, it can be defined as the distance to the maximum thermicity, where the thermicity is a measure of the rate of heat release. In general for ideal gases, the thermicity is defined by,

$$\dot{\sigma} = \sum_n \left(\frac{\tilde{W}}{\tilde{W}_n} - \frac{\tilde{h_n}}{\tilde{C}_p \tilde{T}} \right) \frac{dY_n}{d\tilde{t}}. \tag{14}$$

where $\tilde{C}_p$ is the mixture specific heat at constant pressure, $\tilde{W}$ the mean molar mass, and $\tilde{h}$ is the specific enthalpy. For the three-step chemical kinetic model it reduces to,

$$\dot{\sigma} = (\gamma - 1) \frac{Q}{c^2} \frac{\mathrm{d}z}{\mathrm{d}t}. \tag{15}$$

2.2.2 Effective activation energy

An effective activation energy is defined dimensionally as,

$$E_{\mathrm{a}} = \frac{\tilde{E}_{\mathrm{a}}}{\tilde{R}\tilde{T}_0}. \tag{16}$$

It describes the sensitivity of the induction time to a thermodynamic perturbation and therefore indicates the mixture stability, where a lower value of E_{a} corresponds to a more stable mixture. Schultz and Shepherd [pp. 81-94, 21] have calculated E_{a} for a wide variety of combustible mixtures. A global Arrhenius form for the induction time is assumed, given by,

$$\tilde{\tau_i} = A \exp\left(\frac{\tilde{E}_{\mathrm{a}}}{\tilde{R}\tilde{T}} \right). \tag{17}$$

Two initial temperatures corresponding to shocks at $\pm 1\%$ the CJ detonation velocity are used, and the corresponding constant volume induction times are found. Then, the two induction time and initial temperature pairs are used to solve Eq. 17 for the activation energy. This method was applied to the present three-step and detailed chemical kinetic models. For the detailed chemistry model the Chemkin software [22] was used for the constant volume calculation. For the two-step model, this parameter is simply $\tilde{E}_{\rm I}/\tilde{R}\tilde{T_{\rm vN}} = E_{\rm I}/T_{\rm vN}$.

2.2.3 Thermal energy

The thermal energy release is the energy released by combustion, defined non-dimensionally as,

$$Q = \frac{\tilde{Q}}{\tilde{R}\tilde{T}_0}. \tag{18}$$

For the two-step and three-step chemical kinetic models the present values of $Q = 30$ or 50, with $\gamma = 1.2$, are chosen to give typical CJ (Chapman-Jouguet) detonation Mach numbers of 4.9 or 6.2. For the two-dimensional simulations, $Q = 50$ with $\gamma = 1.2$ was used exclusively. For the detailed chemistry model it is calculated following [21] using,

$$Q = \frac{\tilde{R}_{\rm CJ}\tilde{T}_{\rm CJ}}{\tilde{R}_0\tilde{T}_0}\left(\frac{\gamma_{\rm CJ}}{\gamma_{CJ}-1}\right)\left(1+\frac{\gamma_{\rm CJ}-1}{2}\right) - \left(\frac{\gamma_0}{\gamma_0-1}\right)\left(1+\frac{\gamma_0-1}{2}M_{\rm CJ}^2\right). \tag{19}$$

The Chemkin software [22] was also used for equilibrium calculations to give the CJ detonation properties $\tilde{R}_{\rm CJ}$, $\tilde{T}_{\rm CJ}$, $\gamma_{\rm CJ}$ and $M_{\rm CJ}$.

2.3 Computational methodology

2.3.1 One-dimensional simulations

For the two-step and three-step chemical kinetic models the simulation was based on a uniform Cartesian grid. Strang splitting is used to treat the hydrodynamic and reactive processes separately. The homogeneous PDE was solved using the second-order MUSCL-Hancock scheme with a van Leer slope limiter and a Harten-Lax-van Leer-contact (HLLC) approximate Riemann solver [23]. A CFL (Courant-Friedrichs-Lewy) number of 0.7 was used. A second-order, two-stage Runge-Kutta method was used for the respective reaction ODEs. The code was validated by comparison to the results in [14, 17]. In both cases a minimum resolution of 100 cells per unit length was used. However, convergence has been verified with resolutions of 200-400 computational cells, and the majority of the presented results utilize the highest resolution.

For the detailed reaction mechanism the problem was simulated using the AMROC framework (Adaptive Mesh Refinement in Object-Oriented C++), developed by Deiterding [24, 25]. The numerical scheme is the second-order MUSCL-TVD scheme with a Roe-type solver, a van-Albada limiter, and Godunov dimensional and source term splitting. In addition, AMROC employs the block-structured adaptive mesh refinement (SAMR) of Berger and Colella [26]. The coarsest grid has 100 cells per cm (10 cells per mm), and four additional levels of refinement are allowed with refinement factors of 2, 2, 4 and 4, respectively. The resolution at the highest level is therefore 640 cells per mm, or $\Delta\tilde{x} = 1.6$ μm. With the range of initial pressures used, this resolution corresponds to 128-1240 cells per ZND induction length. Nevertheless, a resolution test was performed where the base resolution was increased to 200 cells, which gives about 256 points per ZND induction length at minimum.

In all cases the left boundary condition was transmissive. To begin the simulation the incident ZND detonation was placed on the grid at the left of the domain, and the inert layer was placed ahead of it as shown in Fig. 1**(a)**. The thickness of the inert layer, $\delta_{\rm i}$, was increased in steps of approximately two ZND induction lengths until failure was obtained. For high activation energies, the incident detonation may be an unstable pulsating detonation. To handle these cases, different incident detonation strengths were considered by changing the location of the inert layer. This ensemble of simulations result in a larger range of critical thicknesses, and has been included in the error bars for this data.

2.3.2 Two-dimensional simulations

The simulation was based upon a uniform Cartesian grid, and the Strang splitting method was adopted to treat separately the hydrodynamic process and the reactive process. The MUSCL-Hancock scheme with the van Leer non-smooth slope limiter and a Harten-Lax-van Leer-contact (HLLC) approximate solver [23] was used. This numerical scheme is thus of second-order accuracy in space and time (in smooth regions). Graphic-processing-unit-enabled parallel computing was used to accelerate the calculation of the fluxes across the intercell boundaries

and reaction rates. This GPU-enabled simulation code has been validated [27, 28] and used in a series of fundamental studies [29–32] on the propagation and re-initiation dynamics of gaseous detonations.

The domain height in the vertical, y-direction was 300 ZND induction lengths. A periodic boundary condition was applied to the top and bottom boundaries of the domain, and the left and right boundaries were transmissive. The resolution was 10 cells per ZND induction length, but a resolution test was performed at double resolution (20 cells per ZND induction length). To begin the simulation the incident cellular detonation was allowed to fully develop, and then the inert layer was placed ahead of it as in Fig. 1**(a)**. The thickness of the inert layer, $\delta_{\rm i}$, was increased in steps of 50 ZND induction lengths until failure was obtained.

3 Results and Discussion

3.1 Transmission into an infinitely long inert layer

First consider the one-dimensional problem. In this section, typical results with the three-step chemical kinetic mechanism are presented. Consider first the transmission of the detonation wave into the inert medium. Figure 2 shows the flowfield pressure and thermicity at selected times. The initial boundary between reactive and inert gas is at $x = 0$, and the shaded regions define the inert gas. Figure 2**(a)** shows the incident ZND detonation just prior to entering the inert gas. The leading shock is at the von Neumann value, and behind the shock is the induction zone. At the end of the induction, the thermicity rises rapidly and the pressure drops in the reaction zone.

In Fig. 2**(b)**, the detonation has entered the inert gas. Since the gas behind the shock front is moving in the positive x direction, the inert gas will be advected with the shock. Consequently, the shocked inert gas is compressed to a thin region within the induction zone, and the reactive gas from upstream still fills the reaction zone. Therefore, the reaction zone of the ZND detonation is unchanged, and the energy release maintains the leading shock amplitude at the von Neumann value.

In Fig. 2**(c)** and **(d)**, the inert gas enters the reaction zone, and the energy release decreases. Thus, the pressure behind the leading shock decreases and the shock decays continuously. The shock decay begins at about $x = 7$, and the burnout of the reactive gas is completed at about $x = 20$. It is thus of importance to note that even after the detonation enters the inert layer, the mixture behind the leading shock continues to react and the energy release contributes to maintain the shock and slow its decay. Afterward, in Fig. 2**(e)**, the shock continues to decay due to the expansion behind it. Eventually, a constant velocity shock will be obtained. The analytic solution for this final transmitted shock has been obtained by previous researchers [33–35].

3.2 Transmission into downstream reactive gas

Now consider the wave transmission into the downstream reactive gas. Figure 3 shows the leading shock pressure for the detonation transmission across inert layers of different thicknesses, $\delta_{\rm i}$. The y-axis is the leading shock pressure normalized by the von Neumann shock pressure and the x-axis is the shock location. The upstream boundary of the inert layer is at $x = 0$, indicated by the vertical dashed line.

As shown in Fig. 3, the initial decay of the shock follows the case where the inert layer is infinitely long ($\delta_{\rm i} = \infty$ case from Fig. 2). In general, when the shock reaches some lower amplitude, the downstream mixture begins to react and the decay slows. The energy release supports the shock so that the shock amplitude remains more or less constant. During this "quasi-steady" period, the fluctuations are a consequence of pressure waves generated by non-steady energy release of the mixture behind the shock.

If $\delta_{\rm i} \leq 8$, the shock is accelerated to form an overdriven detonation (as indicated on the dotted curve in Fig. 3). It then decays asymptotically, and the characteristic ZND detonation is re-formed. In such a case, a detonation is successfully re-initiated in the downstream reactive gas. If $\delta_{\rm i} \geq 10$, no acceleration of the shock is observed (note that the simulation was run up to a shock location $x_{\rm shock} > 1000$). Such a case is considered as a failure of detonation re-initiation in the downstream reactive gas. Thus, one can determine a critical value of the inert layer thickness for a successful re-initiation in a given reactive mixture. For the mixture with the three-step kinetics considered in this section, the critical thickness is equal to $\delta_{\rm i,cr} = 9 \pm 1$. The transient processes for cases with a successful re-initiation and a failure of re-initiation are demonstrated in detail in the following two subsections, i.e., Sects. 3.2.1 and 3.2.2, respectively.

3.2.1 Successful re-initiation

First consider near-critical case where the detonation is successfully re-initiated downstream, with inert thickness $\delta_{\rm i} = 8$. Figure 4**(a)** shows the normalized pressure and thermicity, while Fig. 4**(b)** shows the normalized tempera-

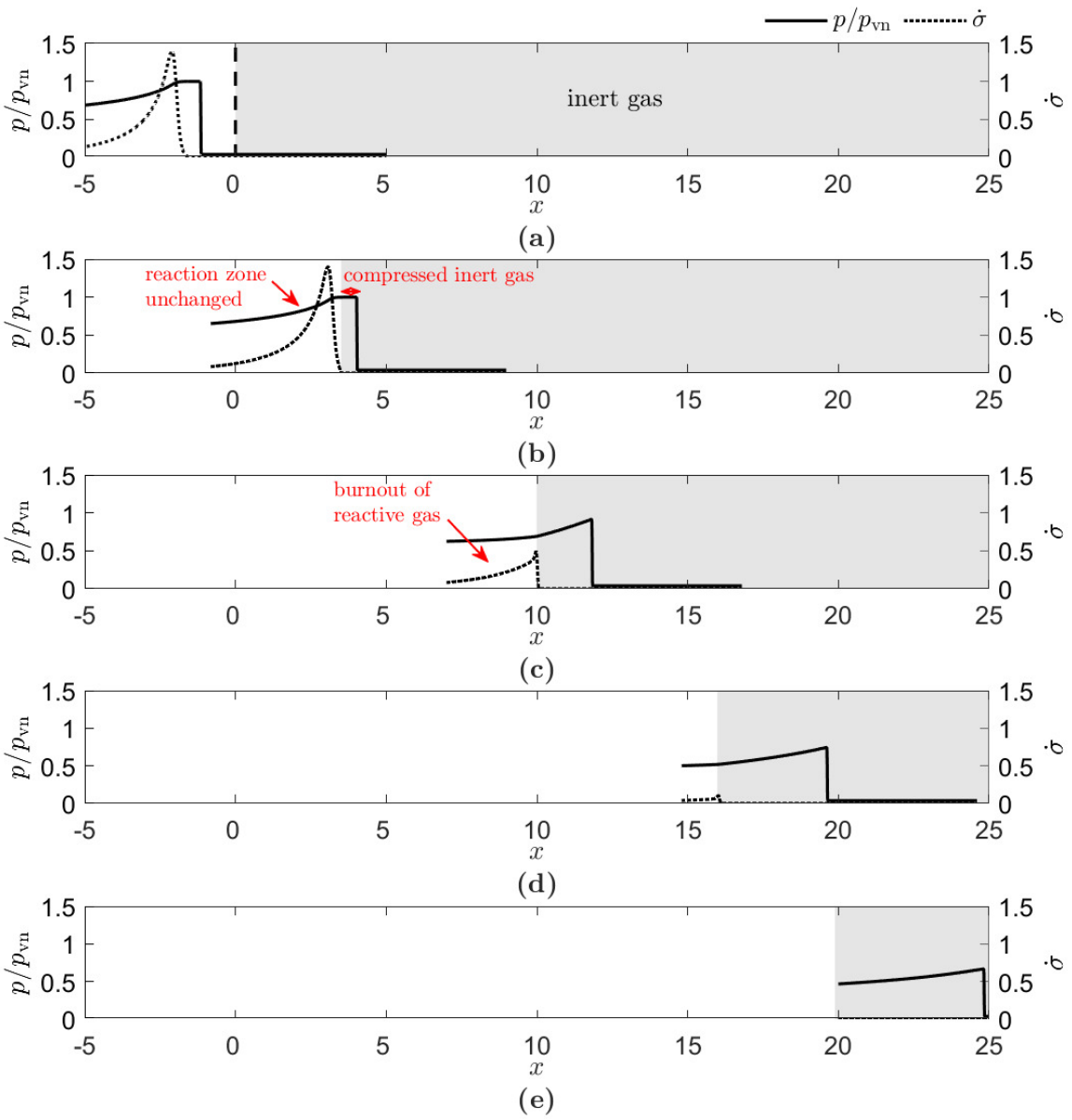

Figure 2: The flowfield pressure normalized by the von Neumann state ($p/p_{\rm vN}$), and the thermicity ($\dot{\sigma}$), for detonation transmission into the inert gas ($\delta_{\rm i} = \infty$) at $t = 20.2, 20.3, 22.9, 24.6$ and 25.9, where $\gamma = 1.2$, $\gamma Q = 30$, $E_B = 10$ and $T_B = 0.95 T_{\rm vN}$.

ture and mass fraction of the radical species at selected times. The first profile is the incident ZND detonation, and again the vertical dashed line is the upstream boundary of the inert layer at $x = 0$.

Upon transmission across the inert layer, the transmitted shock is decaying. Near $x = 20$, ignition of the downstream reactive gas can be observed, shown by a new exothermic peak ($\dot{\sigma}$) as indicated in Fig. 4. The energy release impedes the decay and enables the shock to quasi-stabilize. During the quasi-steady period (also labeled in Fig. 3), the reaction front is not coupled to the shock and lags behind. However, the energy release generates small pressure pulses, one of which can be seen near $x = 50$. These pulses propagate forward to temporarily strengthen the shock, and are responsible for the fluctuation of the shock during the quasi-steady period (as was seen in Fig. 3).

When the shock amplitude fluctuates, a disturbance is created in the temperature of the shocked particles. This disturbance is seen afterward in the induction zone of the temperature profiles near $x = 70$. A new reaction front forms at this disturbance near $x = 90$ as indicated in Fig. 4, creating a second peak in temperature, radical species, and exothermicity in front of the original reaction zone. The energy release at the new reaction front increases rapidly, and an accompanying pressure pulse coupled to the reaction front is formed. The coupled pressure pulse

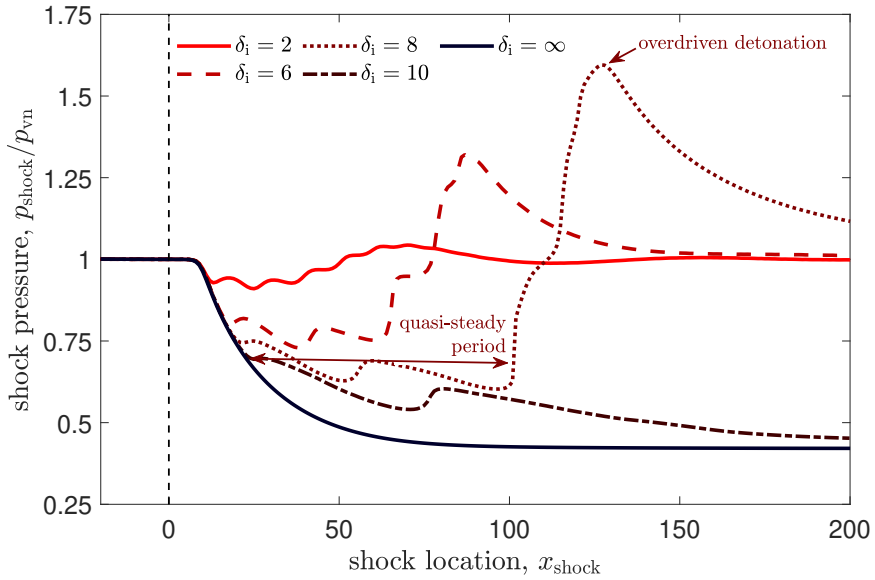

Figure 3: The leading shock pressure normalized by the von Neumann shock pressure ($p_{\rm shock}/p_{\rm vN}$) against the shock location ($x_{\rm shock}$) for inert thicknesses $\delta_{\rm i}$ = 2-10 and $\delta_{\rm i} = \infty$, where $\gamma = 1.2$, $\gamma Q = 30$, $E_B = 10$ and $T_B = 0.95T_{\rm vN}$.

and reaction front are amplified simultaneously, and the front of the pressure pulse steepens to form a new shock. The pulse-shock complex catches up to the transmitted leading shock, and gives rise to the onset of detonation. The original reaction front burns out. When the two shocks collide a contact surface is formed near $x = 110$, at which the right side has a higher temperature. The process repeats, in that a new reaction front forms at the contact surface. The energy release at the new reaction front leads to further pressure increase and a more strongly overdriven detonation. Again, the original reaction front burns out.

The onset of detonation is analyzed in more detail via a distance-time (x-t) diagram as shown in Fig. 5. The solid black line is the leading shock front. The red dashed lines are the reaction fronts, which are defined as the trajectory of the maximum thermicity, i.e., $\dot{\sigma}_{\rm max}$. Finally, the black dotted lines are representative u+c characteristics. In addition, profiles of pressure and $\dot{\sigma}$ are shown again for reference, at selected times indicated by the grey arrows.

In the first profile at $t = 40.5$ (shown in Fig. 5), the new reaction front is forming ahead of the original reaction front. The energy release at the new front is smaller than at the original reaction front. In this region of the x-t diagram, both reaction fronts are receding, i.e. progressively decoupling, from the shock front. In the second profile at $t = 41.75$, the energy release at the new reaction front has increased to become larger than that at the original front. Simultaneously, in this region of the x-t diagram, the new reaction front is abruptly accelerated toward the shock. Notice that the reaction front becomes briefly parallel to the u+c characteristic at this location, which is shown by a thicker line for emphasis. Therefore, when this characteristic compresses the gas ahead of the reaction front its reaction is intensified, driving the reaction front forward. Henceforth, the energy release and pressure pulse are mutually amplified; the energy release amplifies the pressure pulse, and in turn compression of the gas by the pulse intensifies the reaction. This mutual amplification is evident in the last two profiles at $t = 43.5$ and $t = 44.75$. Simultaneously, the original reaction front burns out. In addition, the front of the pressure pulse is steepening into a shock, as observed in the last profile and the convergence of the characteristics at the top right of the x-t diagram.

3.2.2 Failure of re-initiation

Consider now a case where the detonation fails to re-initiate downstream, with an inert thickness $\delta_{\rm i} = 10$, which is shown in Fig. 6. In this case the process initially proceeds as before. The decaying leading shock ignites the downstream reactive mixture at $x = 30$; however, the reaction front lags behind the shock. Nevertheless, a small pressure pulse is formed at $x = 75$ which catches up to the shock. The fluctuation in shock amplitude creates a temperature disturbance in the induction zone near $x = 100$. At the temperature disturbance, a new reaction front develops near $x = 150$. However, contrary to the "go" case, there is no rapid increase in reaction rate or pressure

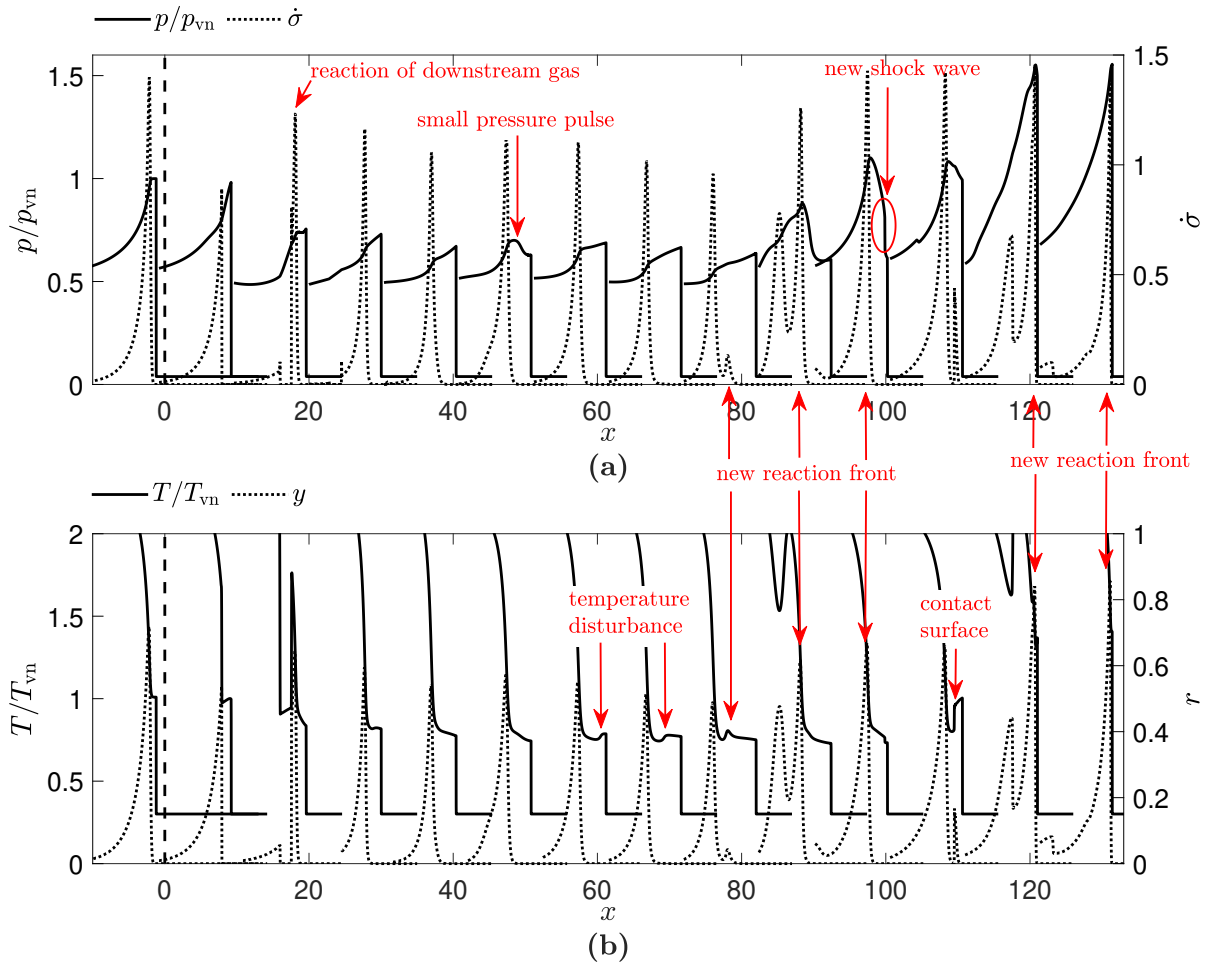

Figure 4: **(a)** The flowfield pressure normalized by the von Neumann state ($p/p_{\rm vN}$), and the thermicity ($\dot{\sigma}$) **(b)** The flowfield temperature normalized by the von Neumann state ($T/T_{\rm vN}$), and radical species mass fraction (r), for inert thickness $\delta_{\rm i} = 8$, where $\gamma = 1.2$, $\gamma Q = 30$, $E_B = 10$ and $T_B = 0.95 T_{\rm vN}$.

at the new reaction front. In the last profile, the pressure pulse is decoupled from the reaction front, and thus, insufficiently effective to maintain the shock strength.

3.3 Effect of chemical kinetics on the critical thickness

The critical thickness was found for the three chemical kinetic models and their corresponding parameters. The results are plotted in Fig. 7, where the y-axis is the critical thickness, $\delta_{\rm i,cr}$ normalized by the ZND induction length, $\Delta_{\rm I}$. The x-axis is the effective activation energy, $E_{\rm a}$. In this plane the data lie on a curve, shown by the dashed line. Points below (or to the left of) the curve constitute transmission success, whereas points above (or to the right of) the curve constitute transmission failure. For the cases with $E_{\rm a} \lesssim 24$, a distinct critical thickness cannot be found. Thus, the dashed line is extended towards infinity beyond this point. Nevertheless, activation energies below 24 are generally unrealistic for detonable mixtures.

Overall, the critical thickness is shown to be dependent on the mixture parameters $\Delta_{\rm I}$ and $E_{\rm a}$ only, regardless of the chemical kinetic model. In general, the detonability of a mixture is dependent on both a characteristic length scale such as the cell size, and the mixture stability which can be manifested for example by the cell regularity [9–11]. In the present study, the characteristic length scale is $\Delta_{\rm I}$, and the mixture stability is captured by $E_{\rm a}$.

Furthermore, it can be seen that the critical thickness ranges from the order of magnitude of the ZND induction length to an order of magnitude larger. It is worth noting that the critical thickness obtained in the one-dimensional numerical study of Wang *et al.* [7] was $0.15\,\mathrm{mm}$, which is similar in magnitude to those obtained in the present study. However, the critical thicknesses obtained in the experiments of Bull *et al.* [1] and Bjerketvedt *et al.* [2], are of the order of $\delta_{\rm i,cr} \sim 100\,\mathrm{mm}$ or 100 $\Delta_{\rm I}$. Therefore, the one-dimensional simulations under-predict the critical

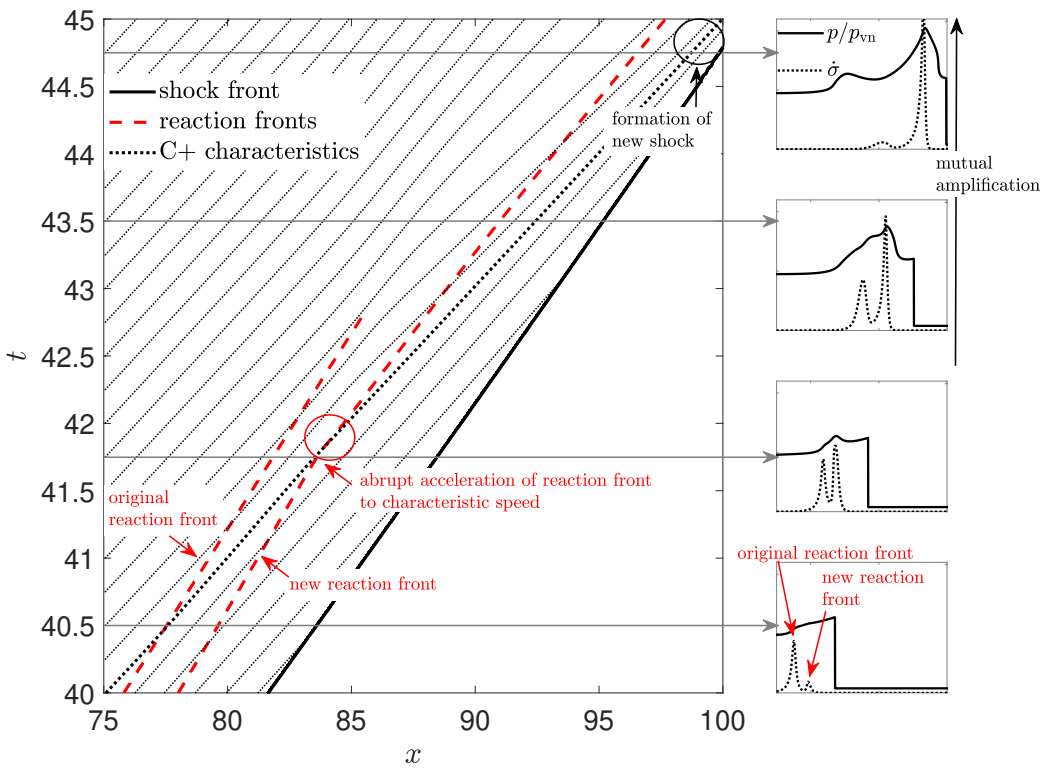

Figure 5: Distance-time (x-t) diagram and the normalized pressure (p/p_{vN}) and thermicity ($\dot{\sigma}$) flowfield at $t = 40.5, 41.75, 43.5, 44.75$, for the pressure pulse at the end of the quasi-steady period with inert thickness $\delta_{\mathrm{i}} = 8$, where $\gamma = 1.2$, $\gamma Q = 30$, $E_B = 10$ and $T_B = 0.95 T_{\mathrm{vN}}$.

thickness by at least an order of magnitude. This discrepancy is likely due to the transverse wave instabilities that are present in multi-dimensional gaseous detonations. Collision of the transverse waves can create similar reaction spots with higher exothermicity, assisting in detonation onset and extending the critical thickness.

Finally, the incident ZND detonation has been assumed to be followed by combustion products at a constant thermodynamic state. This setup represents an idealized case of an infinitely long tube. More generally, an expansion wave referred to as a Taylor wave trails behind the detonation, further expanding the combustion products. In such a case, the transmitted shock would decay further to an acoustic wave, at a rate depending on the characteristics of the Taylor wave. Therefore, the amplitude of the transmitted shock at some given inert thickness may decrease, and so the critical thickness may decrease. In particular, for the mixtures with very low E_{a} to the left of the vertical line in Fig. 7, a critical thickness could be found if the Taylor wave were included. Therefore, the present results can be considered as an upper bound for the critical thickness.

3.4 Two-dimensional simulations

Typical numerical sootfoils for a two-dimensional simulation are shown in figure 8, where the inert layer thicknesses are $\delta_{\mathrm{i}} = 100$, 150, and 200 in figures 8**(a)**, 8**(b)**, and 8**(c)**, respectively. These numerical sootfoils were created by tracking the maximum pressure in the domain. The vertical dashed lines indicate the boundaries of the inert layer. The incident detonation cellular structure is fairly unstable with an irregular cell pattern. When the detonation enters the inert layer, as with the one-dimensional case, there is a reduction in the energy release from chemical reactions and the detonation decays. The strength of the shock front decreases overall, including the transverse waves. For the inert thicknesses of 100 and 150, the detonation re-initiates downstream of the inert layer at the collision of the transverse waves. Therefore, the transverse waves provide the re-initiation mechanism in two-dimensions. The detonation cannot be re-initiated when $\delta_{\mathrm{i}} = 200$, so the critical thickness is 175 ± 25.

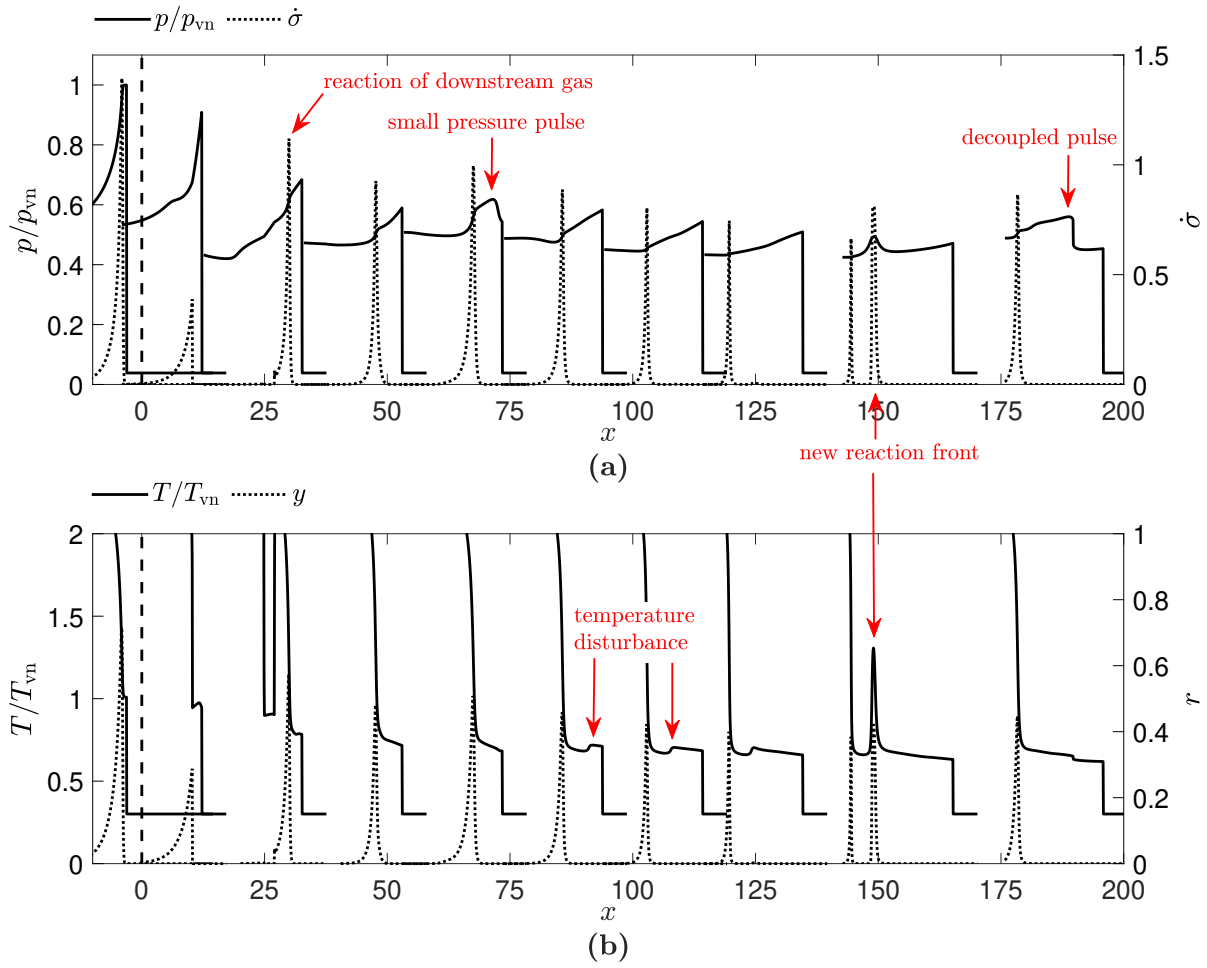

Figure 6: **(a)** The flowfield pressure normalized by the von Neumann state ($p/p_{\rm vN}$), and the thermicity ($\dot{\sigma}$) **(b)** The flowfield temperature normalized by the von Neumann state ($T/T_{\rm vN}$), and radical species mass fraction (r), for inert thickness $\delta_{\rm i} = 10$, where $\gamma = 1.2$, $\gamma Q = 30$, $E_B = 10$ and $T_B = 0.95 T_{\rm vN}$.

3.4.1 Comparison of critical thicknesses

For the two-dimensional simulations, 10 runs were performed for each $E_{\rm a}$ and an average critical thickness, $\delta_{\rm i,cr}$ was calculated. The results are plotted in figure 9, where the x-axis is the activation energy $E_{\rm a}$, and the y-axis is $\delta_{\rm i,cr}/\Delta_{\rm I}$. The experimental results of Bull *et al.* [1] for ethylene-air and propane-air are also plotted for comparison. When the resolution is increased $\delta_{\rm i,cr}$ appears to decrease, which may be explained by a change in numerical diffusion. Numerical diffusion can aid in detonation re-initiation [36]; therefore, with higher resolution and less diffusion detonation initiation may become more difficult.

The average critical thicknesses obtained in the two-dimensional simulations are of the same order of magnitude as the experiment results of Bull *et al.* [1]. Moreover, the same trend of decreasing critical thickness with increasing $E_{\rm a}$ is obtained. Nevertheless, any discrepancies could potentially be explained by two factors. In experiments, diffusive effects will create a zone of variable composition at the boundaries of the inert layer. In the present study, diffusive effects were ignored in order to create well-defined boundaries and eliminate this complexity. In addition, the present study has assumed no change in thermodynamic state from reactive to inert gas (i.e. no change in shock impedance). In a previous study [3], the transmission of a detonation wave across an interface with a change in thermodynamic state was investigated. The focus of the current study is placed upon probing the effects of the energetics only. These two simplifications may be a source of discrepancy between the numerical and experimental results.

It is also worthwhile to again compare with the numerical study of Wang *et al.* [7]. These authors reported a two-dimensional critical thickness of $0.37\,\mathrm{mm}$ for a series of inert layers with spacing of $2\,\mathrm{mm}$, which is still smaller than the present results and experimental results in [1]. However, since this result is for a series of inert

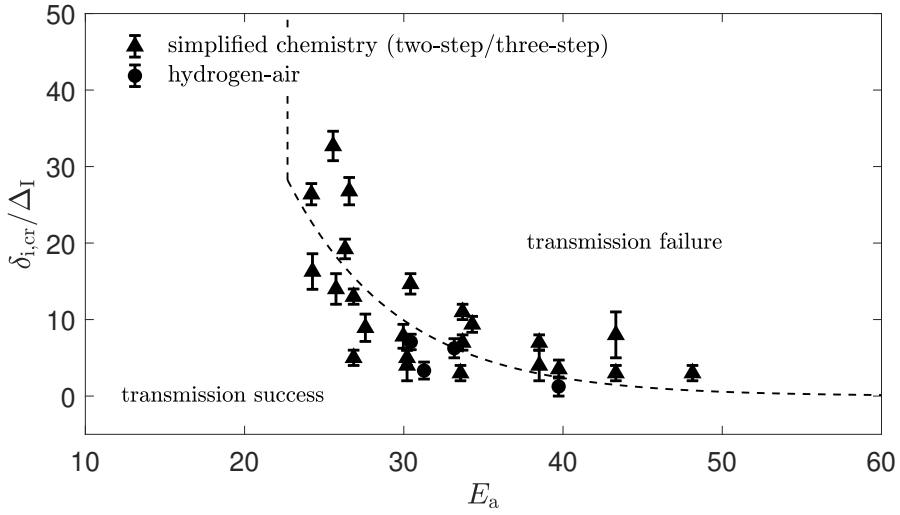

Figure 7: The critical inert thickness ($\delta_{\mathrm{i,cr}}$) normalized by the ZND induction length (Δ_{I}) against the effective activation energy (E_{a}), for all chemical kinetic models and parameters.

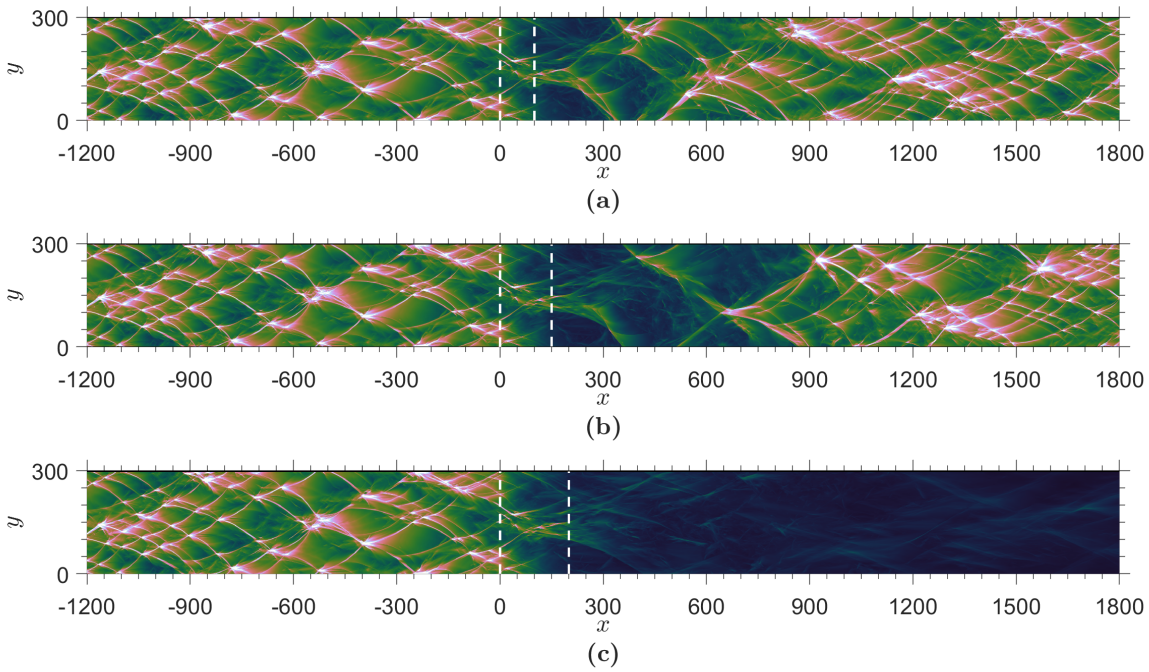

Figure 8: Numerical sootfoils for inert thicknesses **(a)** $\delta_{\mathrm{i}} = 100$, **(b)** $\delta_{\mathrm{i}} = 150$, and **(c)** $\delta_{\mathrm{i}} = 200$, where $E_{\mathrm{I}} = 9T_{\mathrm{vN}}$.

layers the problems are not identical. In addition, the reactive mixtures considered here ($E_{\mathrm{a}} \sim$ 43–63) and in the experiments in [1] (ethylene-air and propane-air) are unstable. On the other hand, the hydrogen mixture considered by Wang *et al.* is relatively stable with a regular cellular structure. Such stable mixtures are known to have multidimensional structures closer to the idealized one-dimensional ZND model [17]. Thus, the difference between one and two-dimensions may be less pronounced.

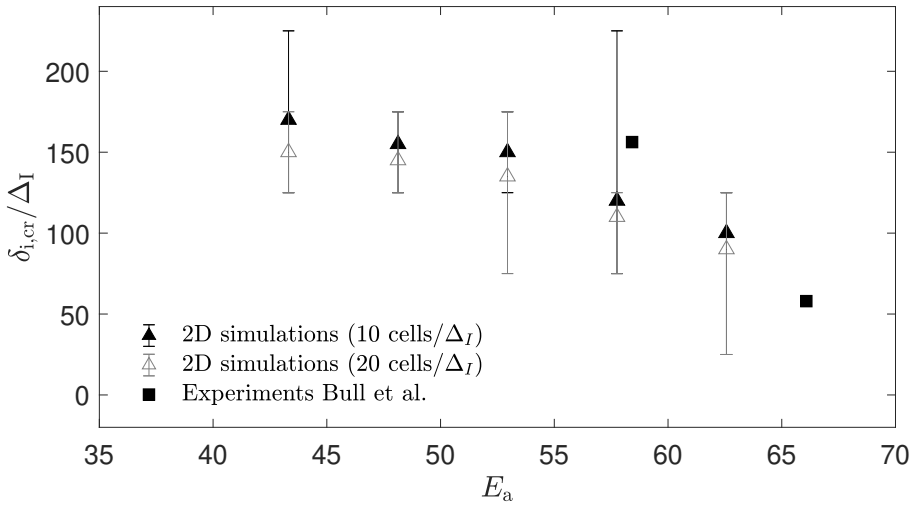

Figure 9: The critical inert thickness ($\delta_{\mathrm{i,cr}}$) normalized by the ZND induction length (Δ_{I}) against the effective activation energy (E_{a}), for the two-dimensional numerical simulations, and the experiments of Bull *et al*. [1].

4 Concluding remarks

In the present study, the transmission of a detonation wave across a layer of inert gas has been examined via one-dimensional and two-dimensional numerical simulations. In one-dimension, a decaying shock is transmitted into the reactive gas downstream of the inert layer. This transmitted shock is sufficiently strong to trigger reactions in the downstream gas, and the resulting energy release generates pressure pulses. During the quasi-steady period, the pressure pulses are not coupled to the energy release, so they remain small and propagate ahead of the reaction front. Nevertheless, they support the shock and allow it to quasi-stabilize at a relatively low speed. At the end of the quasi-steady period, the pressure pulses may couple to the energy release. The critical process was found to be the acceleration of the reaction front to the characteristic speed. This coupling leads to a rapid amplification of the energy release and of the pressure pulse, resulting in an acceleration of the transmitted shock and the onset of detonation. In two-dimensions, the detonation re-initiates at the collision of the transverse waves.

The critical thickness is the thickness of the inert layer above which the detonation cannot be re-initiated downstream. A parametric study has shown that the one-dimensional critical thickness, $\delta_{\mathrm{i,cr}}$, can be adequately described by the ZND induction length, Δ_{I}, and an effective activation energy, E_{a}. The one-dimensional simulations, however, under-predict previous experimental results [1, 2] by at least an order of magnitude. This discrepancy is resolved by adding another dimension. With two-dimensions, transverse wave instabilities are present and allow detonation re-initiation in cases where it was not possible in one-dimension. This multi-dimensional re-initiation will be further explored in future work.

Acknowledgements

Kelsey Tang-Yuk was supported by the Fonds de recherche du Québec - Nature et technologies, file number 270439.

References

[1] D.C. Bull, J.E. Elsworth, M.A. McLeod, D. Huges, Initiation of Unconfined Gas Detonations in Hydrocarbon-Air Mixtures by a Sympathetic Mechanism, Gasdynamics of Detonations and Explosions 75 (1979) 61–72.

[2] D. Bjerketvedt, O.K. Sonju, I.O. Moen, The Influence of Experimental Condition on the Reinitiation of Detonation Across an Inert Region, Dynamics of Explosions 106 (1986) 109–130.

[3] K.C. Tang Yuk, X.C. Mi, J.H.S. Lee, H.D. Ng, Transmission of a detonation across a density interface, Shock Waves 28 (2018) 967–979.

[4] T. Engebretsen, D. Bjerketvedt, O.K. Sonju, Propagation of Gaseous Detonations Through Regions of Low Reactivity, Dynamics of Explosions 153 (1993) 324–346.

[5] T.P. Gavrilenko, A.N. Krasnov, Y.A. Nikolaev, Transfer of a gas detonation through an inert gas "plug", Combust. Explo. Shock 18 (1982) 240–244.

[6] A. Teodorczyk, F. Benoan, Interaction of detonation with inert gas zone, Shock Waves 6 (1996) 211–223.

[7] Y. Wang, R. Deiterding, Z. Chen, Propagation of gaseous detonation across inert layers, Proc. Combust. Inst. 38 (2021) 3555–3563.

[8] D. Tropin, I. Bedarev, Physical and mathematical modeling of interaction of detonation waves with inert gas plugs, J. Loss Prevent. Proc 72 (2021).

[9] I. Moen, A. Sulmistras, G.O. Thomas, D. Bjerketvedt, P.A. Thibault, Influence of cellular regularity on the behavior of gaseous detonation, Dynamics of Explosions 106 (1986) 220–243.

[10] D. Desbordes, C. Guerraud, L. Hamada, H.N. Presles, Failure of the Classical Dynamic Parameters Relationships in Highly Regular Cellular Detonation Systems, Dynamic Aspects of Detonations 153 (1993) 347–359.

[11] M.I. Radulescu, G.J. Sharpe, D. Bradley, A universal parameter for quantifying explosion hazards, detonability and hot spot formation, the χ number, in: D. Bradley, G. Makhviladze, V. Molkov, P. Sunderland, F. Tamanini (Eds.), Seventh International Seminar on Fire and Explosion Hazards, Research Publishing (2013) 617—626.

[12] J.W. Dold, A.K. Kapila, Comparison between shock initiations of detonation using thermally sensitive and chain-branching chemical models, Combust. Flame 85 (1991) 185–194.

[13] M. Short, J. Quirk, On the nonlinear stability and detonability limit of a detonation wave for a model three-step chain-branching reaction, J. Fluid Mech 339 (1997) 89–119.

[14] H. D. Ng, J.H. Lee, Direct initiation of detonation with a multi-step reaction scheme, J. Fluid Mech 476 (2003) 179–211.

[15] P.A. Blythe, A.K. Kapila, M. Short, Homogeneous ignition for a three-step chain-branching reaction model, J. Eng. Math 56 (2006) 105–128.

[16] C.K. Law, Combustion Physics. Cambridge university press, Cambridge, UK, 2006.

[17] H.D. Ng, M.I. Radulescu, A.J. Higgins, N. Nikiforakis, J.H. Lee, Numerical investigation of the instability for one-dimensional Chapman-Jouguet detonations with chain-branching kinetics, Combust. Theor. Model 9 (2005) 385-–401.

[18] C. Leung, M. I. Radulescu, G. J. Sharpe, Characteristics analysis of the one-dimensional pulsating dynamics of chain-branching detonations, Phys. Fluids 22 (2010).

[19] Y. E. Poroshyna, A. I. Lopato, P. S. Utkin, Nonlinear dynamics of pulsating detonation wave with two-stage chemical kinetics in the shock-attached frame, J. Inverse Ill-pose P (2020).

[20] C.K. Westbrook, Chemical kinetics of hydrocarbon oxidation in gaseous detonations, Combust. Flame 46 (1982) 191–210.

[21] E. Schultz, J. Shepherd, Validation of Detailed Reaction Mechanisms for Detonation Simulation, Report No. FM99-5, California Institute of Technology, Graduate Aeronautical Laboratories, Pasadena, CA, USA, 2000.

[22] R.J. Kee, F.M. Rupley, J.A. Miller, Chemkin-II: a Fortran chemical kinetics package for the analysis of gas-phase chemical kinetics, Report No. SAND-96-8216, Sandia National Laboratories, Livermore, CA, USA, 1996.

[23] E.F. Toro, Riemann Solvers and Numerical Methods for Fluid Dynamics, Springer-Verlag, Berlin, 1997.

[24] R. Deiterding, A parallel adaptive method for simulating shock-induced combustion with detailed chemical kinetics in complex domains, Comput. Struct 87 (2009) 769–783.

[25] R. Deiterding, Parallel Adaptive Simulation of Multi-dimensional Detonation Structures, PhD thesis, Brandenburgische Technische Universität Cottbus (2003).

[26] M.J. Berger, P. Colella, Local adaptive mesh refinement for shock hydrodynamics, J. Comput. Phys 82 (1989) 64–84.

[27] G. Morgan, The Euler equations with a single-step Arrhenius reaction, M.S. thesis, University of Cambridge (2013).

[28] C. Kiyanda, G. Morgan, N. Nikiforakis, H. D. Ng, High resolution gpu-based flow simulation of the gaseous methane-oxygen detonation structure, J. Visual-Japan 18 (2015) 273-–276.

[29] X. C. Mi, A. J. Higgins, H. D. Ng, C. B. Kiyanda, N. Nikiforakis, Propagation of gaseous detonation waves in a spatially inhomogeneous reactive medium, Physical Review Fluids 2 (2017).

[30] X. Mi, A. Higgins, C. Kiyanda, H. Ng, N. Nikiforakis, Effect of spatial inhomogeneities on detonation propagation with yielding confinement, Shock Waves 28 (2018) 993—1009.

[31] H. Xu, X. Mi, C. B. Kiyanda, H. D. Ng, J. H. Lee, C. Yao, The role of cellular instability on the critical tube diameter problem for unstable gaseous detonations, Proc. Combust. Inst. 37 (2019) 3545–3553.

[32] C. Yan, H. Teng, X. Mi, H. D. Ng, The effect of chemical reactivity on the formation of gaseous oblique detonation waves, Aerospace 6 (2019) 62.

[33] R.B. Morrison, A shock tube investigation of detonative combustion, Report No. UMM-97, Willow Run Research Center, University of Michigan, MI, USA, 1952.

[34] S. Paterson, Contact transmission of detonation, Symp. (Int.) Combust. 4 (1953) 468–471.

[35] J.T. Peace, F.K. Lu, Detonation-to-shock wave transmission at a contact discontinuity, Shock Waves 28 (2018) 981–992.

[36] M. I. Radulescu, A detonation paradox: Why inviscid detonation simulations predict the incorrect trend for the role of instability in gaseous cellular detonations?, Combust. Flame 195 (2018) 151–162.